Since January 2020 Elsevier has created a COVID-19 resource centre with free information in English and Mandarin on the novel coronavirus COVID-19. The COVID-19 resource centre is hosted on Elsevier Connect, the company's public news and information website.

Journal of Environmental Management 289 (2021) 112522

Contents lists available at ScienceDirect

Journal of Environmental Management

journal homepage: http://www.elsevier.com/locate/jenvman

Research article

Imprints of COVID-19 lockdown on the surface water quality of Bagmati river basin, Nepal

Ramesh Raj Pant [a], Kiran Bishwakarma [b,c], Faizan Ur Rehman Qaiser [d,*], Lalit Pathak [a], Gauri Jayaswal [a], Bhawana Sapkota [a], Khadka Bahadur Pal [e], Lal Bahadur Thapa [f], Madan Koirala [a], Kedar Rijal [a], Rejina Maskey [a]

[a] Central Department of Environmental Science, Institute of Science and Technology, Tribhuvan University, Nepal
[b] Key Laboratory of Tibetan Environment Changes and Land Surface Processes, Institute of Tibetan Plateau Research, Chinese Academy of Sciences, Beijing, 100101, China
[c] University of Chinese Academy of Sciences, Beijing, 100049, China
[d] Department of Earth Sciences, COMSATS University Islamabad, Abbottabad Campus, Pakistan
[e] Tri-Chandra Multiple Campus, Tribhuvan University, Kathmandu, Nepal
[f] Central Department of Botany, Institute of Science and Technology, Tribhuvan University, Nepal

ARTICLE INFO

Keywords:
COVID-19 pandemic
Lockdown
Chemical characterization
Organic pollution
Water quality
Bagmati river

ABSTRACT

COVID-19 pandemic has caused profound impacts on human life and the environment including freshwater ecosystems globally. Despite the various impacts, the pandemic has improved the quality of the environment and thereby creating an opportunity to restore the degraded ecosystems. This study presents the imprints of COVID-19 lockdown on the surface water quality and chemical characteristics of the urban-based Bagmati River Basin (BRB), Nepal. A total of 50 water samples were collected from 25 sites of BRB during the monsoon season, in 2019 and 2020. The water temperature, pH, electrical conductivity, total dissolved solids, dissolved oxygen (DO), and turbidity were measured in-situ, while the major ions, total hardness, biological oxygen demand (BOD), and chemical oxygen demand (COD) were analyzed in the laboratory. The results revealed neutral to mildly alkaline waters with relatively moderate mineralization and dissolved chemical constituents in the BRB. The average ionic abundance followed the order of $Ca^{2+} > Na^{+} > Mg^{2+} > K^{+} > NH_4^{+}$ for cations and $HCO_3^{-} > Cl^{-} > SO_4^{2-} > NO_3^{-} > PO_4^{3-}$ for anions. Comparing to the pre-lockdown, the level of DO was increased by 1.5 times, whereas the BOD and COD were decreased by 1.5 and 1.9 times, respectively during the post-lockdown indicating the improvement of the quality water which was also supported by the results of multivariate statistical analyses. This study confirms that the remarkable recovery of degraded aquatic ecosystems is possible with limiting anthropic activities.

1. Introduction

The world has faced the deadly COVID-19 pandemic, an infectious disease caused by severe acute respiratory syndrome coronavirus 2 (SARS-CoV-2); firstly reported in December 2019 in Wuhan, China (Dennison Himmelfarb and Baptiste, 2020; Franch-Pardo et al., 2020). It has affected >215 countries across the world and declared a Global Health Emergency on January 30th, 2020 by World Health Organization (Lai et al., 2020). In order to reduce the pace of spreading this contagious virus via personal contacts, several countries have imposed different modalities of nationwide lockdown. Meanwhile, nearly half of the global population was under strict lockdown and normal life had come to a standstill as a result of the pandemic (Shah et al., 2020). There were numerous negative impacts imposed by cluster lockdown in social and economic wellbeing which cannot be appreciated at all but it appeared that the degraded ecosystems are rejuvenating under the lockdown period and the quality of the environment has been improving noticeably (Chaurasia et al., 2020).

The pandemic directly impacted the whole global commnity, which could have irreparable environmental repercussions. Globally, the lockdown hit micro-enterprises, tourism, business, transport, entertainment, and most importantly, the survival and livelihoods of poor and

* Corresponding author.
E-mail address: faizan@cuiatd.edu.pk (F.U. Rehman Qaiser).

https://doi.org/10.1016/j.jenvman.2021.112522
Received 22 October 2020; Received in revised form 13 March 2021; Accepted 29 March 2021
Available online 10 April 2021

disadvantaged groups of people (Murugesan et al., 2020). Despite those negative consequences, the lockdown reduced anthropic pressure on different spheres of the environment, thereby improving their quality throughout the globe to some extent (Pinder et al., 2020; Islam et al., 2020; Mahato et al., 2020). For instance, the degraded ecosystems were restored in terms of air, water, and natural habitats (Corlett et al., 2020). The severely polluted hydrosphere is exclusively a problem that arises due to the direct disposal of domestic and municipal sewerage, rapid urbanization, industrialization, and overexploitation of natural resources (Mishra et al., 2017). The ecological functions of the aquatic environment are being jeopardized by a multitude of human-mediated stressors (Diamantini et al., 2018). Recent studies revealed that the pollution levels have been decreased significantly in the heavily contaminated freshwater ecosystems under the lockdown period (Shah et al., 2020; Yunus et al., 2020). For instance, the Ganges and Mandakini Rivers (India) reflected a notable recovery of the water quality during the lockdown phase (Dutta et al., 2020; Chaurasia et al., 2020).

In the case of Nepal, the first COVID-19 case was confirmed on January 23, 2020 (the first recorded case in South Asia), and the Government of Nepal had announced the lockdown on March 24, 2020 and extended it to July 22, 2020. It had greatly impacted the normal functioning of daily life, including societal and economic aspects. Despite several negative issues due to the lockdown, the vehicular emissions and industrial sources of pollution had also been paused and therefore, it was expected that the level of pollution might have reduced in the environment, particularly in the urban-based river systems. The Bagmati River is the lifeline and major source of water supply in the core urban area of Nepal and downstream regions and also one of the heavily polluted urban-based river systems. Thus, this study has attempted to evaluate the recovery and imprints of COVID-19 lockdown on the surface water quality in the Bagmati River Basin (BRB), Nepal.

2. Materials and methods

2.1. Study area

Nepal, a Himalayan country characterized by plenty of freshwater resources, is situated between India and China. The study was carried out in the Bagmati River that drains through the core urban area of Nepal. It lies between 26°42′ - 27°50′ N and 85°02′ - 85°58′ E, covering a catchment area of 3756 km^2 (Fig. 1). The river originates from the Shivapuri Hill (2650 m.a.s.l.), flowing to a distance of >25 km within the core urban area (196 km within Nepal) and eventually joins the Ganges River in India (Mishra et al., 2017; Thakur et al., 2017). There are 24 tributaries including Bishnumati and Manahara feeding to the Bagmati River Basin (BRB). The average precipitation in the basin is ~1400 mm/year where approximately 80% of the annual precipitation occurs during the monsoon season from June to September (Panthi et al., 2015). The average discharge of the river is 10.67 m^3/s with the highest value of 35.15 m^3/s during the monsoon season (Bhatt et al., 2014). Geologically, the headwater of the river basin contains mica gneiss and biotite schist with muscovite, whereas the middle segment is characterized by unconsolidated clay, silt, sand, and gravels. The downstream is mainly comprised of fine-grained phyllite, slates, limestone, shales, quartz, and mudstones (Mehta and Rana, 2018).

The land use along the BRB is mainly characterized by forest, agricultural land, and built-up area. The upstream, midstream, and downstream segments of the BRB are covered by forest, core built-up area, and agricultural land, respectively. . The land use pattern of BRB is forest > agriculture > built-up > grassland > barren land > water bodies (Fig. A1). Meanwhile, there are three major cities viz. Kathmandu, Lalitpur, and Bhaktapur with population density 19,726 people/sq.km, 14,574 people/sq.km, and 2662 people/sq.km, respectively in the midstream segment of the BRB (Lamichhane and Shakya, 2020).

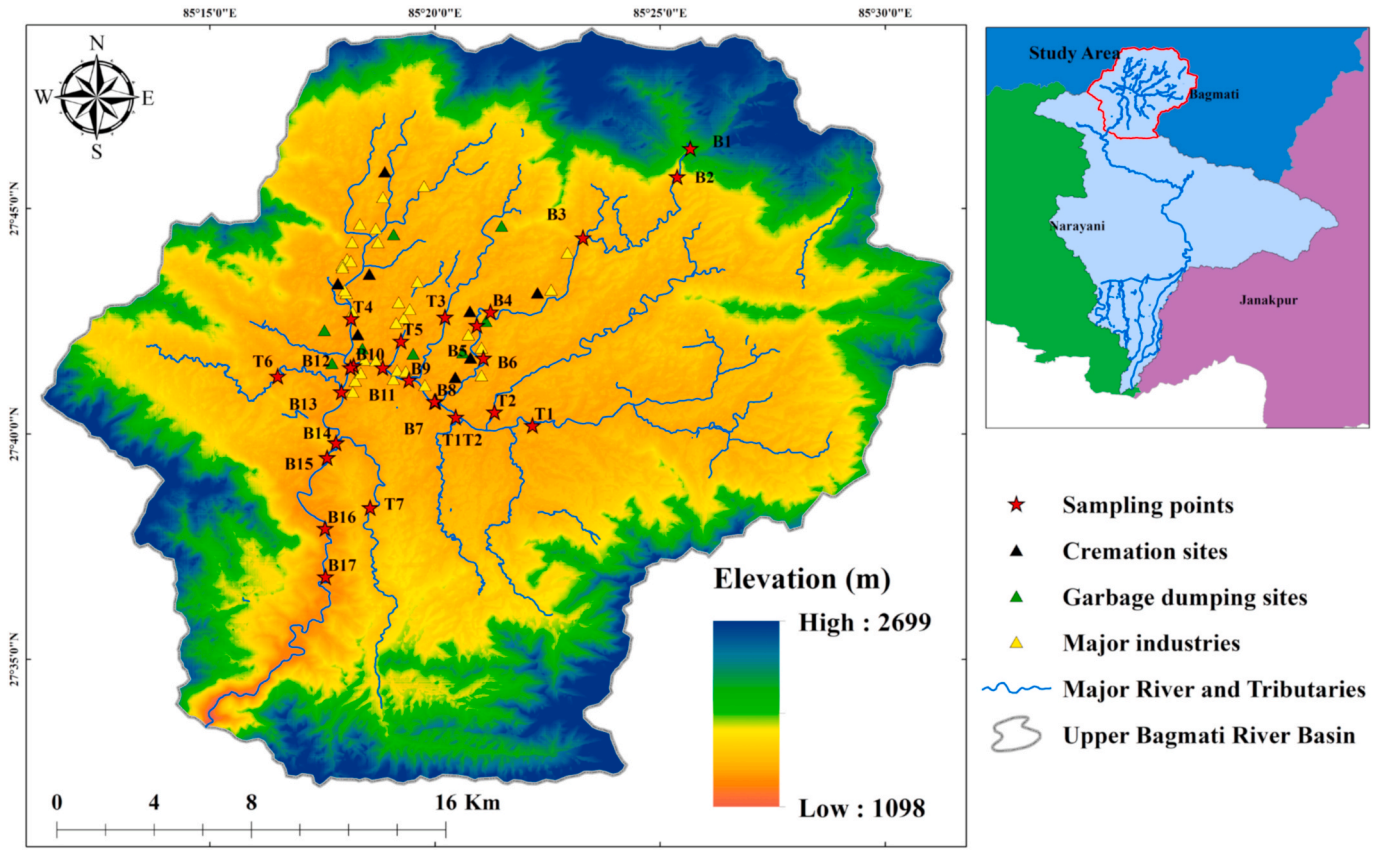

Fig. 1. Sampling locations in the Bagmati River Basin (BRB), Nepal.

Additionally, more than 2.3 million people are living in the middle segment of the basin with an annual population growth rate of 4.63% (CBS, 2011).

2.2. Sampling design and chemical analysis

In this study, the water samples were collected from the main river and tributaries of the BRB (Fig. 1). A total of 50 water samples were collected (8 from the tributaries and 42 from the main river) in the two consecutive years i.e., 2019 and 2020 during the monsoon season (July). The samples were taken from both banks and the center of the main river and tributaries and mixed thoroughly for making the composite sample at each of the sampling points. Considering the sampling situation of 2019, the sampling of 2020 was conducted to maintain the rainfall and flowrate consistent. Importantly, the water samples were taken on the days without rainfall in 24 h to control the relatively compatible condition of discharge. The samples were collected from a depth of 20−30 cm below the surface of the water body using wide-mouth high-density polyethylene (HDPE) bottles of 1 L, which were rinsed with the same river water twice before the sampling.

In-situ measurements were carried out for the water temperature, pH, electrical conductivity (EC), total dissolved solids (TDS) using a multi−parameter probe HANNA, whereas dissolved oxygen (DO) was measured by using DO Meter. The determination of suspended particulate matters was done by using WAGERTECH Turbidity Meter. The samples were filtered using a 0.45 μm milli-pore nitrocellulose filter and the filtrate was collected in 20 mL HDPE bottles. Furthermore, the samples for cation analysis were preserved by acidification with 2 M HNO_3, and the bottles were packed inside the double polyethylene zip-lock bags. The samples were transported to the Central Department of Environmental Science, Institute of Science and Technology, Tribhuvan University, Nepal for laboratory analysis.

The chemical parameters such as total hardness (TH), alkalinity, biological oxygen demand (BOD), chemical oxygen demand (COD), major cations (Ca^{2+}, Mg^{2+}, K^+, Na^+, NH_4^+), and major anions (Cl^-, NO_3^-, SO_4^{2-}, PO_4^{3-}, HCO_3^-) were analyzed using the standard methods prescribed by APHA (2005). The concentrations of Na^+ and K^+ were determined by using Microprocessor Flame Photometer, ESICO MODEL 1382. Similarly, the determination of NO_3^-, SO_4^{2-}, PO_4^{3-}, and NH_4^+ were carried out by using SSI UV 2101 Spectrophotometer. SO_4^{2-} was measured by the Gravimetric method using $BaCl_2$ crystals whereas, the EDTA titration was used for the Ca^{2+}, Mg^{2+}, HCO_3^- and TH. Additionally, Cl^- was determined by the Argentometric method using K_2CrO_4 as an indicator (Pal et al., 2019). Likewise, the open-air reflux method and 5-day BOD-test were performed to determine the level of COD and BOD, respectively. For quality control, non-powder vinyl cleanroom gloves and masks were used during sample collection and laboratory work to avoid contamination. The collected samples were stored in a refrigerator at 4 °C until the laboratory tasks were performed.

2.3. Statistical analyses and interpretations

Descriptive statistics were performed to evaluate and interpret the hydrochemical variations of the dataset. The relationship between the hydrochemical parameters was examined by using correlation analysis. As the data did not obey Gaussian distribution, Spearman's rho correlation analysis was applied using Statistical Package for the Social Sciences (IBM SPSS Statistics version 26.0). The student t-test was applied to compare the parameters between the years 2019 and 2020. The data of the tributaries and the main river were analyzed separately.

Hierarchical cluster analysis (HCA) based on Ward's method with Euclidean distances was applied with the intent of grouping similar sampling sites (Varol et al., 2013). Meanwhile, the principal component analysis (PCA) was applied to identify the sources of the hydrochemical variables. In order to account for the degree of mutually shared variability between individual pairs of hydrochemical parameters, the correlation matrix was determinant whereas the multiplication of correlated parameters was estimated by eigenvalues. The first eigenvalue represented the greatest variation among the observed parameters and the subsequent values provided the proportionately smaller contributions (Zeng and Rasmussen, 2005). The eigenvalue >1 was considered to assess the significant associations among the chemical parameters, and the dataset was standardized using varimax rotation. The validity and effectiveness of PCA in reducing the dimensionality of the dataset were tested using the Kaiser-Meyer-Olkin (KMO) test and Bartlett's sphericity methods (Singh et al., 2004; Qaisar et al., 2018).

The Piper diagram (Piper, 1944) and mixing plots were used for the chemical characterization of hydrochemical variables. Besides, the suitability of river water for irrigation purposes was evaluated by sodium percentage (Na%) (Doneen, 1954), sodium adsorption ratio (SAR) (Richards, 1954), magnesium hazard (MH) (Raghunath, 1987), Kelly's ratio (KR) (Ibraheem and Khan, 2017), permeability index (PI) (Joshi et al., 2009), cation ratio of soil structural stability (CROSS) (Rengasamy and Marchuk, 2011) and Wilcox diagram (Wilcox, 1955). The water quality index (WQI) was applied to evaluate the river water quality for drinking purposes (Sahu and Sikdar, 2008). Also, the potable nature of water was examined by comparing it to the WHO standards (WHO, 2011). The details of the WQI and irrigation quality assessment were explained elsewhere (Acharya et al., 2020).

3. Results and discussion

3.1. General hydrochemistry

The descriptive statistics of hydrochemical compositions of the BRB (pre-lockdown and post-lockdown) are presented in Table 1. The mildly alkaline pH value in the BRB indicated the mixed type (both carbonate and silicate) of underlying lithology. The pre-lockdown TDS value of 563 mg/L decreased to 227 mg/L during post-lockdown, suggesting the markedly high anthropic pollution in the urban segments. Comparing to the global average i.e., 120 mg/L (Gaillardet et al., 1999), the TDS values were 4.69 and 1.89 times higher during pre-lockdown and post-lockdown periods, respectively (Table 1). Generally, the TDS values were found to be < 120 mg/L in most of the freshwater rivers, but the higher values observed even in post lockdown could be due to municipal wastes and agricultural runoff in the BRB (Pal et al., 2019; Paudyal et al., 2016). Also, the EC dropped from 956 μS/cm to 431 μS/cm, indicating substantially less dissolved materials in the river water during post-lockdown. The turbidity value had noticeably diminished from 206.21 NTU to 124.38 NTU. The dramatic reduction of turbidity during the post-lockdown period indicated a low amount of suspended solids in the river water. A slight decrease in TH was observed from 195.28 mg/L to 144.32 mg/L, also depicting low chemical load during the post-lockdown. The pattern of cationic dominance based on mean values (mg/L) in the BRB was found in the order of $Ca^{2+} > Na^+ > Mg^{2+} > K^+ > NH_4^+$. The Ca^{2+} with Na^+ jointly contributed ~67% and 72% of the total cationic budget during the pre-lockdown and post-lockdown, respectively. The excessive concentration of Na^+ might be due to the silicate rock weathering near the source region of the river (B1) (Bhatt et al., 2014). Although the concentration of NH_4^+ was found to be the lowest among the measured cations, its average value was higher as compared to the other Himalayan river basins (Table A3). Furthermore, the order of the anionic concentrations based on the mean values was found in the order of $HCO_3^- > Cl^- > SO_4^{2-} > NO_3^- > PO_4^{3-}$. The dominant anion in the BRB was HCO_3^- which accounts for 64% followed by Cl^- with 30% during pre-lockdown, and 52%, and 42% during post-lockdown, respectively. The higher level of the Cl^- concentration as compared to other river systems of Nepal (Table A3) could be due to the sewage discharge and agricultural runoff (Bhatt et al., 2007). The concentrations of NO_3^- and SO_4^{2-} were found to be much lower and contributed <5% to the total anionic budget. The PO_4^{3-} was found as the least abundant anion throughout the basin with ~1% contribution during

Table 1
Descriptive statistics of the hydrochemical compositions of the Bagmati River Basin, Nepal.

	Pre-Lockdown (n = 25)				Post-Lockdown (n = 25)				Grand Mean[a]	WHO Guideline
	Min	Max	Mean	SD	Min	Max	Mean	SD		
Temp.	9.40	18.20	15.50	2.01	18.50	29.50	24.58	2.35	20.04	–
pH	6.23	9.98	8.09	1.09	4.60	7.99	7.37	0.69	7.73	6.5–8.5
EC	42	1739	956	451	31	912	431	195	693	1500
TDS	31	980	563	278	16	456	227	101	395	1000
Ca^{2+}	17.51	97.45	50.55	18.23	7.20	62.40	36.00	14.35	43.28	100
Mg^{2+}	12.36	17.96	15.54	1.71	0.49	30.26	13.25	8.13	14.40	50
K^{+}	4.80	26.72	13.86	5.00	1.75	20.67	12.02	4.14	12.94	100
Na^{+}	13.78	97.22	44.43	17.97	5.40	108.00	37.39	21.44	40.91	200
NH_4^{+}	0.25	12.14	7.29	2.81	0.09	2.54	1.20	0.64	4.25	–
Cl^{-}	3.35	154.40	73.68	39.09	7.10	100.82	50.21	19.71	61.94	250
NO_3^{-}	0.89	6.57	3.76	1.63	0.27	4.23	2.37	1.14	3.06	50
SO_4^{2-}	0.98	7.56	4.74	1.68	1.54	8.46	3.89	1.78	4.31	250
HCO_3^{-}	43.05	805.65	493.97	226.92	230.00	575.00	402.40	74.19	448.18	600
PO_4^{3-}	0.22	4.82	2.26	1.42	0.19	4.50	1.61	1.18	1.93	–
Tur.[b]	1.50	431.90	206.21	119.15	3.20	350.00	124.38	103.02	165.30	5
TH	80.00	360.00	195.28	62.60	28.00	220.00	144.32	49.89	169.80	500
DO	0.24	8.20	1.59	2.05	1.33	9.47	3.18	2.05	2.39	>4
BOD	2.20	288.00	162.80	79.60	6.40	187.00	95.20	45.76	129.00	<30[c]
COD	6.00	856.00	469.84	236.43	12.00	408.00	217.60	100.83	343.72	<250[c]

{All units are in mg/L except Temperature (°C); EC (μS/cm); Turb. (NTU) and pH}.
[a] Grand mean is estimated as the mean of the two sampling periods (Pre- and post-lockdown, COVID-19).
[b] Tur.: Turbidity.
[c] Indian Drinking water quality standards (BIS, 2012).

pre-lockdown and post-lockdown.

The results indicated that variations in the hydrochemical parameters in the BRB were mainly controlled by the extent of anthropic activities which were also consistent with the previous studies (Paudyal et al., 2016; Pal et al., 2019). It has clearly revealed that the relatively low concentrations of hydrochemical parameters during the post lockdown (Table 1) indicate the imprints of lockdown in the core urban area. The parameters were also compared with selected rivers of Nepal, Asia, and global mean values and found that the EC, TDS, and dissolved ions were relatively higher in the BRB (except SO_4^{2-}) (Table A3).

The hydrochemical parameters in the BRB were compared between the pre-lockdown and post-lockdown (Fig. 2). The parameters were displayed bipolarity with a substantial difference between the samples taken during pre-lockdown and post-lockdown situations. The concentrations of dissolved chemicals in terms of TDS were found to be significantly lower during post-lockdown ($p \leq 0.05$), as compared to the pre-lockdown samples in both river and tributaries (Fig. 2). It might be due to less discharge of pollutants during the post-lockdown period. Overall, the water quality of BRB was found poor as confirmed by the comparison with the WHO guidelines (Table 1).

3.2. Spatiotemporal variations of hydrochemistry

The hydrochemistry of the BRB was found to be varying spatially (main river and tributaries) and temporally (pre-lockdown and post-lockdown) (Fig. 3). All the chemical parameters were reduced in both the main river and tributaries during the post-lockdown period (Fig. 2). Among them, the EC, TDS, Ca^{2+}, Na^{+}, Cl^{-}, and NH_4^{+} were significantly decreased after the lockdown. Interestingly, K^{+} and HCO_3^{-} were significantly diminished only in the tributaries (Fig. 2). This indicates that the reduced amount of effluents from the industries and domestic sectors during the lockdown in the BRB. The results are consistent with the previous studies which have indicated that the discharges from industries and domestic effluents are the major contributors to increase the pollution load in the urban-based river systems (Sada, 2012).

Among the major cations, Ca^{2+} has the highest and NH_4^{+} has the lowest in their concentrations in the basin during both pre-lockdown and post-lockdown (Table 1). Meanwhile, the concentrations Na^{+} and K^{+} were found to be much higher in the core urban area than in the headwater region indicating the intensive anthropic signatures including sewage, chemical fertilizers, and domestic wastes (Fig. 1). On the other hand, the HCO_3^{-} and NO_3^{-} showed the highest and lowest concentrations, respectively among the anions in the BRB. The concentrations of NO_3^{-} exhibited an increasing pattern moving from the

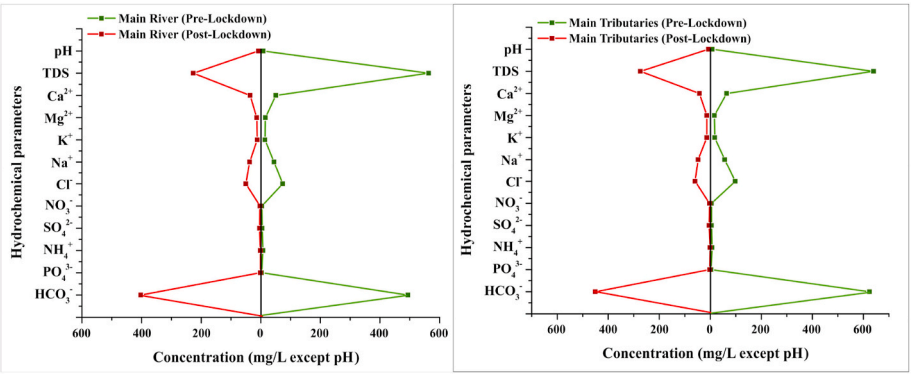

Fig. 2. Variations of hydrochemical parameters during the pre-lockdown and post-lockdown in the main river and tributaries of the Bagmati River Basin (BRB), Nepal.

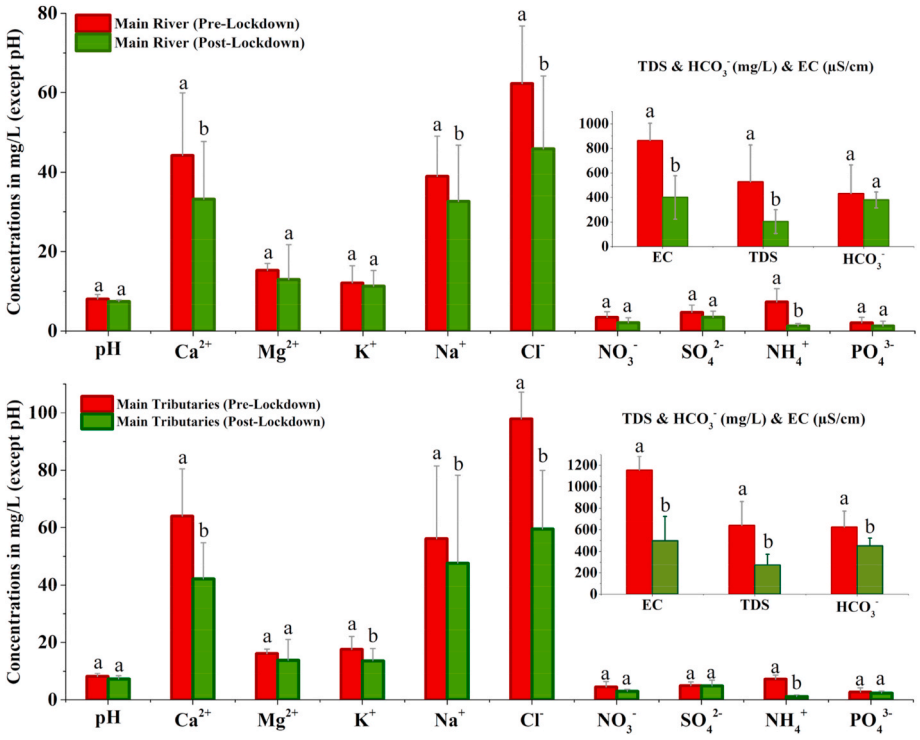

Fig. 3. Temporal variations of hydrochemistry in the (a) main river and (b) tributaries of the Bagmati River Basin (BRB), Nepal. The associated bars represent the standard deviations. The letters above the error bar represent the statistically significant differences in the variables ($p < 0.05$).

headwater region to the core urban area, which could be due to the dense human settlements and intense anthropic inputs (Fig. 1). The Hindu cremation sites are located in the vicinity, which could also be the major input sources of NO_3^- in the river water (Thakur et al., 2017; Pal et al., 2019). Also, the famous Hindu Temple named Pashupatinath is another major source of anthropic contamination in the river segment (Fig. 1). Thousands of pilgrims used to visit and worship Lord Shiva in the area every day which could have a direct impact on the river water quality, however, the lockdown had also limited the activities of pilgrims.

The lower concentration of SO_4^{2-} in comparison to Cl^- in the basin might be due to the natural reduction of sulfate to sulfide in presence of high organic loads (Zhang et al., 2019). The main reason for the relatively low concentration of SO_4^{2-} could be due to low natural inputs as was confirmed from the high pH value in the river water (Pant et al., 2018).

Additionally, the results also exhibited that the tributaries were relatively more contaminated as compared to the main river (Fig. 3) which could be explained as the major contributions of agricultural runoff, discharges from a number of brick industries, and domestic wastewater from the vicinity of densely populated core-urban areas along the tributaries (Fig. 1). In summary, both the spatial and temporal assessments consistently exhibited the marked anthropic signatures, particularly from untreated domestic sewage, agricultural, and industrial effluents in the BRB.

3.3. Variation of DO, BOD, and COD

During the post-lockdown, the anthropic intervention in the river system was limited as a result of lockdown imposition. The level of DO, BOD, and COD varied noticeably at the spatial and temporal levels in the BRB (Table 1 and Fig. 4). The average value of COD and BOD during the post-lockdown period decreased from 469.84 mg/L to 217.60 mg/L (1.9 times) and 162.80 mg/L to 95.20 mg/L (1.5 times), respectively, while the average DO increase from 1.59 mg/L to 3.18 mg/L (~1.5 times)

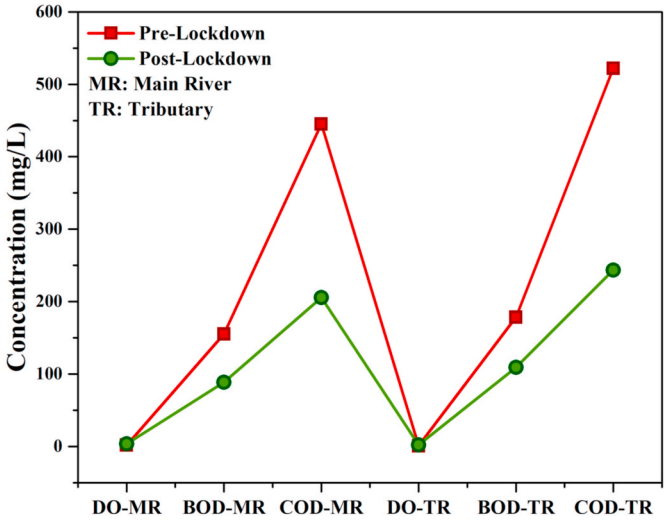

Fig. 4. DO, BOD, and COD illustrating the improvement of water quality during post-lockdown as compared to pre-lockdown in the main river and tributaries of the Bagmati River Basin (BRB), Nepal.

indicating the lesser load of organic pollution in the river system during post-lockdown. The highest values of COD and BOD were observed from the core urban segment of BRB ($p < 0.05$, Table A2). It provides strong evidence of heavy contamination in the water bodies from organic wastes and industrial effluents in the BRB (Mishra et al., 2017). The results confirm that the water quality of BRB has been improved during the lockdown period.

3.4. Characterization of hydrochemical facies

The milli−equivalent percentage (meq %) of major ions was illustrated in the Piper diagram to evaluate the hydrochemical facies and

types of water (Fig. 5). In the cation section, most of the samples lied in the lower center of the triangle, indicating the dominance of Ca^{2+} and $Na^{+}+K^{+}$ (Fig. 5). Meanwhile, a few samples from the tributaries implied relatively higher concentrations of Na^{+} (i.e., T1, T3, and T5). Generally, the local anthropic sources contribute to the elevated concentrations of Na^{+} in the water bodies (Pant et al., 2018). Furthermore, the Ca^{2+} and Mg^{2+} concentrations relatively increased during lockdown might have caused by the lower concentrations of K^{+} and Na^{+} ions. It consistently signifies the reduction of anthropic inputs over geogenic inputs.

On the other hand, the anion section illustrated that most of the water samples during post-lockdown existed on the lower-left corner near the HCO_3^{-} apex (Fig. 5). Nevertheless, the majority of the water samples during pre-lockdown were enriched with Cl^{-} to some extent, validating relatively large anthropic pressure over the BRB. The results plotted in the central diamond field revealed the overall characteristics and facies (Fig. 5). Furthermore, the central diamond depicted that the comparable concentrations of both alkalies (Na^{+}) with alkaline earth metals (Ca^{2+}) while the weak acids (HCO_3^{-}) had relatively higher concentration as compared to the strong acids (Cl^{-} and SO_4^{2-}). However, the concentration of Na^{+} was found higher in the sampling points of B3, B5, B8, and T3 (Table A2), especially during post-lockdown, characterizing the Ca–Na–HCO_3 type of water facies.

In addition, the higher concentrations of Cl^{-} in the core urban areas may be attributed to the solid and liquid wastes from nearby settlements, cremation sites, and religious places (Fig. 1). These findings were in good agreement with the previous studies conducted in the different religious locations of holy rivers, India (Bhatnagar et al., 2016). In summary, the hydrochemistry of the BRB was mainly characterized by the Ca–HCO_3 type. However, a slight change was observed in the hydrochemical facies in the river water samples during pre-lockdown and post-lockdown, which indicated that most of the major ions were influenced by anthropic activities.

3.5. Association among the hydrochemical attributes

In the present study, principal component analysis (PCA) was applied for 13 hydrochemical variables i.e., pH, EC, TDS, and the major ions based on the 50 water samples taken during pre-lockdown and post-lockdown from the BRB (Fig. 6). The KMO and Bartlett's results were obtained as 0.83 and 613.34 (df = 78, $p < 0.00$) during pre-lockdown and 0.74 and 235.61 (df = 78, $p < 0.00$) during post-lockdown, indicating that PCA would be useful in reducing the dimensionality of the dataset. PC factors were classified by their corresponding loading values as >0.75 and 0.50–0.75, which were considered strong and moderate, respectively ,(Pant et al., 2021).

There were two principal components (PCs) identified for the pre-lockdown with eigenvalues >1, which explained about 78.16% of the total variances (Table A4). PC1 accounting for 69.13% of the total variances, had strong positive loading on EC, TDS, Ca^{2+}, Mg^{2+}, K^{+}, Na^{+}, HCO_3^{-}, PO_4^{3-}, Cl^{-} and moderate positive loading on NO_3^{-} and SO_4^{2-}. The co-locations of these variables indicated mixed types of sources. Similarly, PC2 accounted for 9.03% of the total variance, had strong positive loading on pH and moderate loading on NH_4^{+}. The co-location of these variables indicated their common source and was likely to be influenced by domestic and agricultural activities. Only two PCs during pre-lockdown clearly indicated that anthropic sources of pollution in the BRB were the predominant sources for the contamination of river water. For the post-lockdown, four PCs were identified with eigenvalues >1, which explained about 81.22% of the total variances (Table A4). PC1 accounting for 45.54% of the total variances, had strong positive loading on HCO_3^{-}, PO_4^{3-}, and Cl^{-}; and moderate positive loading on EC, TDS, and Ca^{2+}. These co-locations of major dissolved constituents displayed the common natural sources, primarily driven by natural rock weathering. PC2 which accounted for 14.39% of the total variance, had strong positive loading on K^{+}, Na^{+}, and NH_4^{+}. The co-location of these variables in PC2 indicated their common sources and was likely to be influenced by municipal effluents and agricultural runoff. Likewise, PC3 accounted for 12.20% of the total variance, had strong positive loading on pH. Similarly, PC4, which accounted for 9.10% of the total variance, had strong positive loading on Mg^{2+}. Rock weathering in the river basin was the primary source of Mg^{2+}. It was easily distinguishable from the rest of the chemicals which could have some sort of association with silicate deposit in the headwater region of the Shivapuri Hill (Bhatt et al., 2014).

In order to confirm the PCA results, the Correlation Matrix (CM) was analyzed and plotted for pre-lockdown and post-lockdown (Table A5). The EC was strongly correlated with Ca^{2+}, K^{+}, Na^{+}, Cl^{-}, SO_4^{2-}, and PO_4^{3-} during the pre-lockdown while moderately correlated with Ca^{2+}, K^{+}, and Cl^{-} during the post-lockdown exhibited elevated concentrations of major ions. The TH was positively correlated with EC, implying the major role of Ca^{2+} and Mg^{2+} as dissolved solids. During pre-lockdown, Ca^{2+} level in the water body had depicted a positive relationship with EC, SO_4^{2-}, and PO_4^{3-}. This indicated that the Ca^{2+} was present as $CaSO_4$ and $Ca_3(PO_4)_2$. But during post-lockdown, Ca^{2+} showed a moderately positive relationship with Cl^{-}, depicted the presence of $CaCl_2$. During the pre-lockdown and post-lockdown, temperature exhibited a significant negative correlation with DO, revealing that with an increase in water temperature, the metabolic rate of microorganisms also increases, and hence the amount of DO decreases (APHA, 2005).

Additionally, Ca^{2+}–HCO_3^{-} exhibited a significant moderate correlation while the Mg^{2+}–HCO_3^{-} showed a weak positive correlation, thereby indicating a common origin of these ions in both the study periods (Singh et al., 2016). There was a significant positive correlation between Cl^{-} and SO_4^{2-} during pre-lockdown, but the post-lockdown scenario presented a weak correlation, consistently suggesting the imprints of limited anthropic pressures during the lockdown period. The Na^{+}-K^{+} pair had shown a positive correlation during pre-lockdown and post-lockdown in the BRB, which was most preferably attributed to contamination from sewerage, industrial effluents, and fertilizers (Mishra et al., 2017). In the meantime, a strong positive correlation was observed between BOD and COD during pre-lockdown and

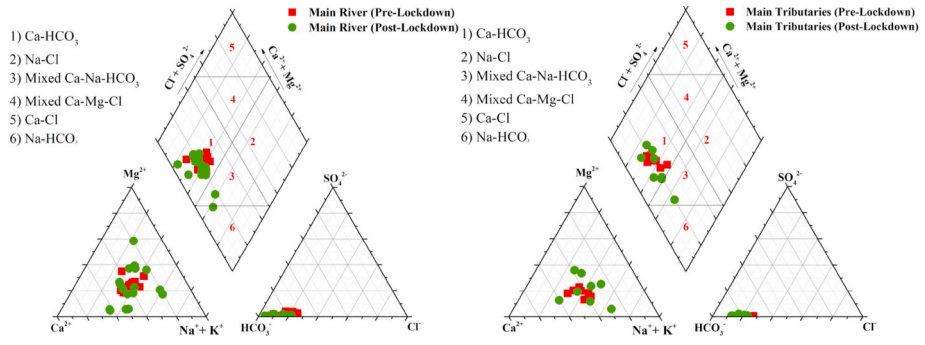

Fig. 5. Piper diagrams showing the relative proportions of major ions (pre-lockdown and post-lockdown) in the main river and its tributaries of the Bagmati River Basin (BRB), Nepal.

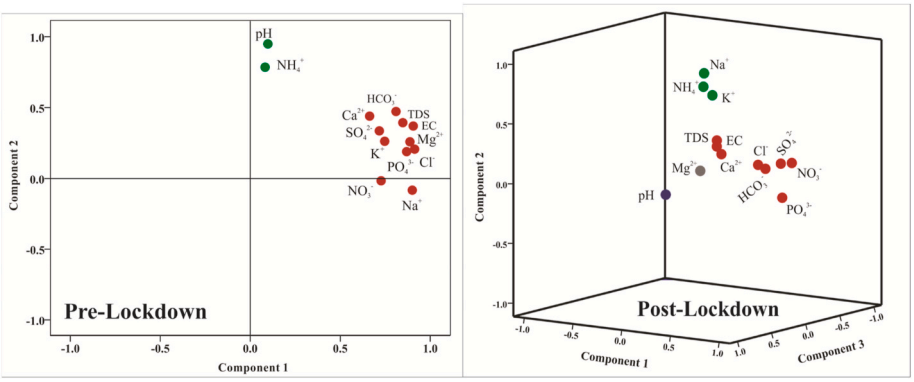

Fig. 6. Principal component analysis (PCA) for pre-lockdown and post-lockdown in the main river and its tributaries of the Bagmati River Basin (BRB), Nepal.

post-lockdown, indicating the excessive loading of organic matters.

The Cluster Analysis (CA) distinguished different statistically significant groups during pre-lockdown and post-lockdown and yielded a dendrogram (Fig. 7). This study generated a total of five clusters during pre-lockdown and most of the sampling points were grouped in clusters A and C (Fig. 7), representing 56% of the total samples. These two clusters included the moderately polluted sampling locations whereas cluster D representing 12% of the total samples (B1, B2, and B3), associated with the headwater pristine region (Sundarijal to Gokarna, Table A1), suggested that the water samples were the least polluted. Cluster B includes mainly the tributaries sampling locations with 16% of the total samples including T1, T4, T5, and B11 (Fig. 7 and Table A1), also corresponded to moderately polluted sampling points and these sections received pollutants from non-point sources. The samples from B4, B5, T2, and T7 formed cluster E, having the highest pollution in the BRB during the pre-lockdown which were mostly attributed to the domestic wastewater and sewerage (Fig. 7 and Table A1).

The clustering pattern was found to be differently allied during post-lockdown (Fig. 7). In this period, four clusters were identified i.e., A, B, C, and D assembling 32%, 12%, 40%, and 16% of the total samples, respectively. Cluster A, C, and D included highly anthropic inputs and polluted sites (Fig. 7, Table A1). Interestingly, a majority of the main river and tributary samples were clustered in Cluster C and D, respectively. Cluster B has the least polluted sites (Fig. 7). The CA results indicated that the water quality of BRB had improved to some extent during post-lockdown with relatively better results from the main river.

3.6. Chemical weathering

To quantify the contribution of rock dissolution and weathering, the ionic ratios of water samples were computed (Table 2). In the present study, the mean molar ratio of HCO_3^-/Ca^{2+} was 4.15 and 5.47 during pre-lockdown and post-lockdown, respectively, confirming that the crucial role of carbonate weathering in the hydrochemistry of the BRB. Similarly, the mean ratios of $(Ca^{2+} + Mg^{2+})/(Na^+ + K^+)$ and $HCO_3^-/(Na^+ + K^+)$ were found to be > 1.5 and > 3 in both the study periods, suggesting the presence of calcite and dolomite minerals in the basin (Table 2). Although the headwater region of BRB is composed of silicate deposits, the hydrochemistry of the core urban area was controlled by carbonate weathering. Meybeck (1987) highlighted that carbonate weathering is 12–40 times faster as compared to silicates, which could be the reason that a very small patch of carbonate deposit can have a greater contribution to the river hydrochemistry of BRB.

The relative importance of proton producing reactions i.e., carbonation and sulfide oxidation in the weathering process can be explained based on $HCO_3^-/(HCO_3^- + SO_4^{2-})$ ratios (C−ratio). The C−ratio <0.5 indicates the chemical reactions of both carbonate dissolution and sulfide oxidation, whereas the ratio ~1 refers absolutely carbonation reactions and dissociation of CO_2 which derives protons from the atmospheric inputs. In the present study, the C−ratios were observed ~1 in both the sampling periods, specifying the significance of carbonate and CO_2 dissolution in proton-producing mechanisms. Additionally, the high ionic ratio of Ca^{2+}/SO_4^{2-} (>25) for pre-lockdown and post-lockdown periods confirmed that H_2SO_4 could not replace H_2CO_3 as a major source of protons for rock weathering in the BRB (Singh et al., 2014). Importantly, the results highlighted relatively a low grand average of Ca^{2+}/Na^+ ratio indicated the higher silicate weathering in the headwater region (Table 2).

The Na^+/Cl^- ratio was >1, which clearly indicated multiple sources of origin including geogenic, anthropic, and atmospheric inputs (Li et al., 2009). The Na^+-normalized pattern of hydrochemistry of the BRB is illustrated in the mixing diagrams (Fig. 8). In the diagrams, most of the samples were located in between the carbonate and silicate end-members showing the contribution of both types of weathering. A few samples were located near the evaporite and silicate end-members (Fig. 8), which specified that the sampling points were likely located near the environments where a high amount of Na^+ and Cl^- ions were present (Fan et al., 2014).

3.7. Water quality index (WQI)

3.7.1. Drinking water quality index (DWQI)

The Bagmati River water is widely used for drinking and other domestic purposes and thus, evaluating its quality is essential. In this study, the WQI has evaluated based on <50, 51–100, 101–200, 201–300, and >300, respectively for excellent, good, permissible, poor, and very poor quality of water (Sahu and Sikdar, 2008; Şener et al., 2017). During the pre-lockdown, the WQI ranged from 13 to 74 and 38 to 87 for the main river and tributaries, respectively indicated that the overall excellent to good water quality. Similarly, during post-lockdown, WQI ranged from 7 to 46 and 30 to 54 for the main river and the tributaries, again indicated overall excellent to good water quality (Table 3).

From the WQI analysis, two insights were highlighting the water quality in the BRB i.e., the main river had relatively better water quality than its tributaries, and overall, the water quality was improved after the lockdown. It can be further confirmed that human activities were limited including industrial effluents entering the rivers due to lockdown. In general, the domestic wastewater discharge in the river should be increased during the lockdown period, however, the scenario of the BRB was contradictory. This could be attributed to the huge mass of the human population (>0.6 million) migrated from the Kathmandu Valley to their original places due to the havoc of the pandemic (Fox et al., 2020).

3.7.2. Irrigation water quality index (IWQI)

As more than 35% area of the BRB is cultivated land, the suitability of river water for irrigation purposes is one of the great concerns from a crop health perspective. From the classification of EC, it was suggested

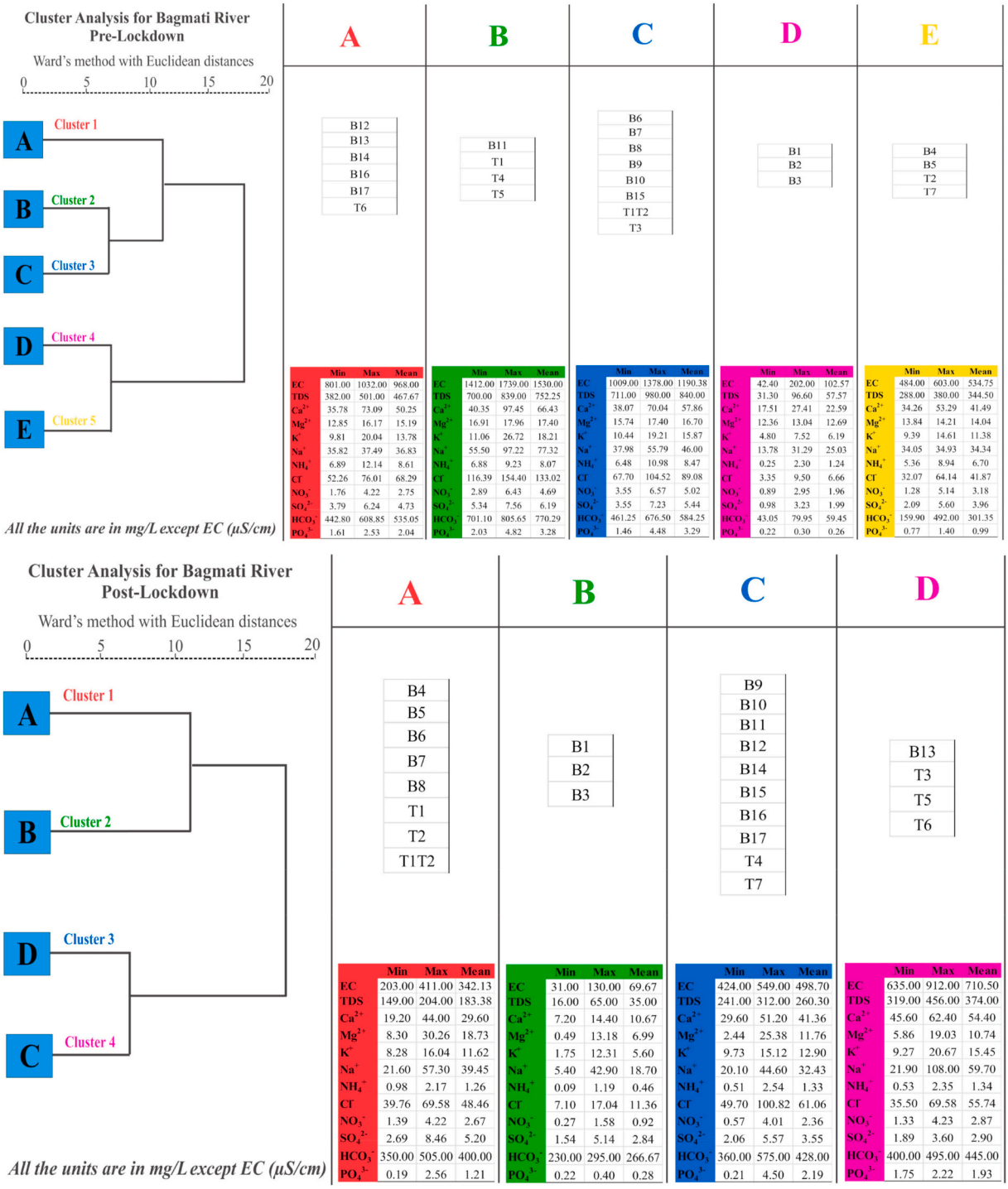

	Min	Max	Mean
EC	801.00	1032.00	968.00
TDS	382.00	501.00	467.67
Ca^{2+}	35.78	73.09	50.25
Mg^{2+}	12.85	16.17	15.19
K^{+}	9.81	20.04	13.78
Na^{+}	35.82	37.49	36.83
NH_4^{+}	6.89	12.14	8.61
Cl	52.26	76.01	68.29
NO_3^{-}	1.76	4.22	2.75
SO_4^{2-}	3.79	6.24	4.73
HCO_3^{-}	442.80	608.85	535.05
PO_4^{3-}	1.61	2.53	2.04

	Min	Max	Mean
EC	1412.00	1739.00	1530.00
TDS	700.00	839.00	752.25
Ca^{2+}	40.35	97.45	66.43
Mg^{2+}	16.91	17.96	17.40
K^{+}	11.06	26.72	18.21
Na^{+}	55.50	97.22	77.32
NH_4^{+}	6.88	9.23	8.07
Cl	116.39	154.40	133.02
NO_3^{-}	2.89	6.43	4.69
SO_4^{2-}	5.34	7.56	6.19
HCO_3^{-}	701.10	805.65	770.29
PO_4^{3-}	2.03	4.82	3.28

	Min	Max	Mean
EC	1009.00	1378.00	1190.38
TDS	711.00	980.00	840.00
Ca^{2+}	38.07	70.04	57.86
Mg^{2+}	15.74	17.40	16.70
K^{+}	10.44	19.21	15.87
Na^{+}	37.98	55.79	46.00
NH_4^{+}	6.48	10.98	8.47
Cl	67.70	104.52	89.08
NO_3^{-}	3.55	6.57	5.02
SO_4^{2-}	3.55	7.23	5.44
HCO_3^{-}	461.25	676.50	584.25
PO_4^{3-}	1.46	4.48	3.29

	Min	Max	Mean
EC	42.40	202.00	102.57
TDS	31.30	96.60	57.57
Ca^{2+}	17.51	27.41	22.59
Mg^{2+}	12.36	13.04	12.69
K^{+}	4.80	7.52	6.19
Na^{+}	13.78	31.29	25.03
NH_4^{+}	0.25	2.30	1.24
Cl	3.35	9.50	6.66
NO_3^{-}	0.89	2.95	1.96
SO_4^{2-}	0.98	3.23	1.99
HCO_3^{-}	43.05	79.95	59.45
PO_4^{3-}	0.22	0.30	0.26

	Min	Max	Mean
EC	484.00	603.00	534.75
TDS	288.00	380.00	344.50
Ca^{2+}	34.26	53.29	41.49
Mg^{2+}	13.84	14.21	14.04
K^{+}	9.39	14.61	11.38
Na^{+}	34.05	34.93	34.34
NH_4^{+}	5.36	8.94	6.70
Cl	32.07	64.14	41.87
NO_3^{-}	1.28	5.14	3.18
SO_4^{2-}	2.09	5.60	3.96
HCO_3^{-}	159.90	492.00	301.35
PO_4^{3-}	0.77	1.40	0.99

	Min	Max	Mean
EC	203.00	411.00	342.13
TDS	149.00	204.00	183.38
Ca^{2+}	19.20	44.00	29.60
Mg^{2+}	8.30	30.26	18.73
K^{+}	8.28	16.04	11.62
Na^{+}	21.60	57.30	39.45
NH_4^{+}	0.98	2.17	1.26
Cl	39.76	69.58	48.46
NO_3^{-}	1.39	4.22	2.67
SO_4^{2-}	2.69	8.46	5.20
HCO_3^{-}	350.00	505.00	400.00
PO_4^{3-}	0.19	2.56	1.21

	Min	Max	Mean
EC	31.00	130.00	69.67
TDS	16.00	65.00	35.00
Ca^{2+}	7.20	14.40	10.67
Mg^{2+}	0.49	13.18	6.99
K^{+}	1.75	12.31	5.60
Na^{+}	5.40	42.90	18.70
NH_4^{+}	0.09	1.19	0.46
Cl	7.10	17.04	11.36
NO_3^{-}	0.27	1.58	0.92
SO_4^{2-}	1.54	5.14	2.84
HCO_3^{-}	230.00	295.00	266.67
PO_4^{3-}	0.22	0.40	0.28

	Min	Max	Mean
EC	424.00	549.00	498.70
TDS	241.00	312.00	260.30
Ca^{2+}	29.60	51.20	41.36
Mg^{2+}	2.44	25.38	11.76
K^{+}	9.73	15.12	12.90
Na^{+}	20.10	44.60	32.43
NH_4^{+}	0.51	2.54	1.33
Cl	49.70	100.82	61.06
NO_3^{-}	0.57	4.01	2.36
SO_4^{2-}	2.06	5.57	3.55
HCO_3^{-}	360.00	575.00	428.00
PO_4^{3-}	0.21	4.50	2.19

	Min	Max	Mean
EC	635.00	912.00	710.50
TDS	319.00	456.00	374.00
Ca^{2+}	45.60	62.40	54.40
Mg^{2+}	5.86	19.03	10.74
K^{+}	9.27	20.67	15.45
Na^{+}	21.90	108.00	59.70
NH_4^{+}	0.53	2.35	1.34
Cl	35.50	69.58	55.74
NO_3^{-}	1.33	4.23	2.87
SO_4^{2-}	1.89	3.60	2.90
HCO_3^{-}	400.00	495.00	445.00
PO_4^{3-}	1.75	2.22	1.93

Fig. 7. The clustering pattern of water samples (pre-lockdown and post-lockdown) in the main river and its tributaries of the Bagmati River Basin (BRB), Nepal.

that IWQI was a "Good" category during pre-lockdown whereas, it was observed as an "Excellent" category during post-lockdown along the tributaries and main river (Table 4). Based on the classification of Na% as excellent <20, good: 20 – 40, permissible: 40 – 60, doubtful: 60 – 80, and unsuitable >80 (Richards, 1954), the water of BRB lay in the excellent to permissible categories.

Similarly, based on the SAR values, irrigation water is classified into four groups (low < 10, medium: 10–18, high: 18 – 26, and very high: > 26) (Saleh et al., 1999; Thomas et al., 2014), with high SAR values indicating increased the risk to the crops. In the BRB, SAR values showed the excellent category (<1.60). Also, based on MH and KR values (<50 and <0.25), the water belonged to the safe category and suitable for irrigation purposes. Likewise, the value of PI was found to be 80.32–107.18 which belonged to Class I, and the CROSS values of the BRB fell under the "Excellent" category (Table 4). Thus, the irrigation water quality of the BRB was safe however, it was suspected that the water quality is deteriorating especially in the tributaries. This could have serious implications for crop productivity in the BRB.

In order to confirm the irrigation water quality results, the Wilcox diagram was applied. It includes four major groups of irrigational water quality namely (i) C1S1, (ii) C1S2, C2S2, C2S1, (iii)C1S3, C2S3, C3S1, C3S2, C3S3, and (iv) C4S4, C4S1, C1S4, C2S4, C3S4, C4S4, C4S3 as

Table 2
Ionic ratios of hydrochemical attributes depicting the pre-lockdown and post-lockdown scenario in the Bagmati River Basin (BRB), Nepal.

Parameter	Pre-lockdown (2019) (n = 25)			Post-lockdown (2020) (n = 25)			Grand mean
	Min	Max	Mean	Min	Max	Mean	
Ca^{2+}/Na^{+}	0.67	2.28	1.36	0.39	2.77	1.33	1.34
Mg^{2+}/Na^{+}	0.35	1.7	0.74	0.1	3.2	0.83	0.78
HCO_3^-/Na^{+}	0.54	6.22	4.15	1.4	16.06	5.47	4.81
HCO_3^-/Ca^{2+}	0.79	6.35	3.11	2.6	13.43	4.37	3.74
$HCO_3^-/(Na^{+}+K^{+})$	0.49	4.82	3.46	1.27	13.49	4.49	3.97
$(Ca^{2+}+Mg^{2+})/(Na^{+}+K^{+})$	1.13	2.84	1.75	0.53	3.53	1.76	1.76
Ca^{2+}/SO_4^{2-}	12.8	61.17	27.59	6.36	79.42	26.64	27.12
Na^{+}/Cl^{-}	0.66	6.5	1.54	0.47	3.89	1.28	1.41
$HCO_3^-/(HCO_3^- +SO_4^{2-})$	0.95	0.99	0.98	0.97	1.00	0.99	0.99
$(Ca^{2+} +Mg^{2+})/Tz^{+}$	0.5	0.74	0.59	0.34	0.78	0.60	0.60
$(Na^{+}+K^{+})/Tz^{+}$	0.26	0.44	0.35	0.22	0.64	0.38	0.36

All ratios derived from μeq, TZ^{+}: the sum of total cations in μeq.Grand mean is estimated as the mean of the two sampling periods (Pre- and post-lockdown, COVID-19).

completely effective for agriculture; brackish-approximate perfect for agriculture; passion-useable for agriculture and very passion-harmful to agriculture, respectively (Alavi et al., 2016; Bishwakarma et al., 2019). Most of the sampling points of the main river and its tributaries fell under C3S1 and C2S1 sections (Fig. 9), indicating the approximate perfection of water for irrigational purposes in the BRB. Moreover, 14% of the total samples were projected in the C1S1 section and considered completely effective for agricultural usages (Fig. 9). Additionally, most of the samples during pre-lockdown were categorized in the C3S1 section i.e., passion category, specifying the useable for agricultural purposes, whereas during the post-lockdown, most of the samples fell under the C2S1 section, indicating approximate perfect water for agriculture purposes.

Table 3
Drinking Water Quality Index (DWQI) depicting the pre-lockdown and post-lockdown scenario in the Bagmati River Basin (BRB), Nepal.

River sections	WQI	Category
Pre-lockdown-main river	47.56	Excellent
Post-lockdown-main river	32.48	Excellent
Pre-lockdown-tributary	63.43	Good
Post-lockdown-tributary	40.56	Excellent

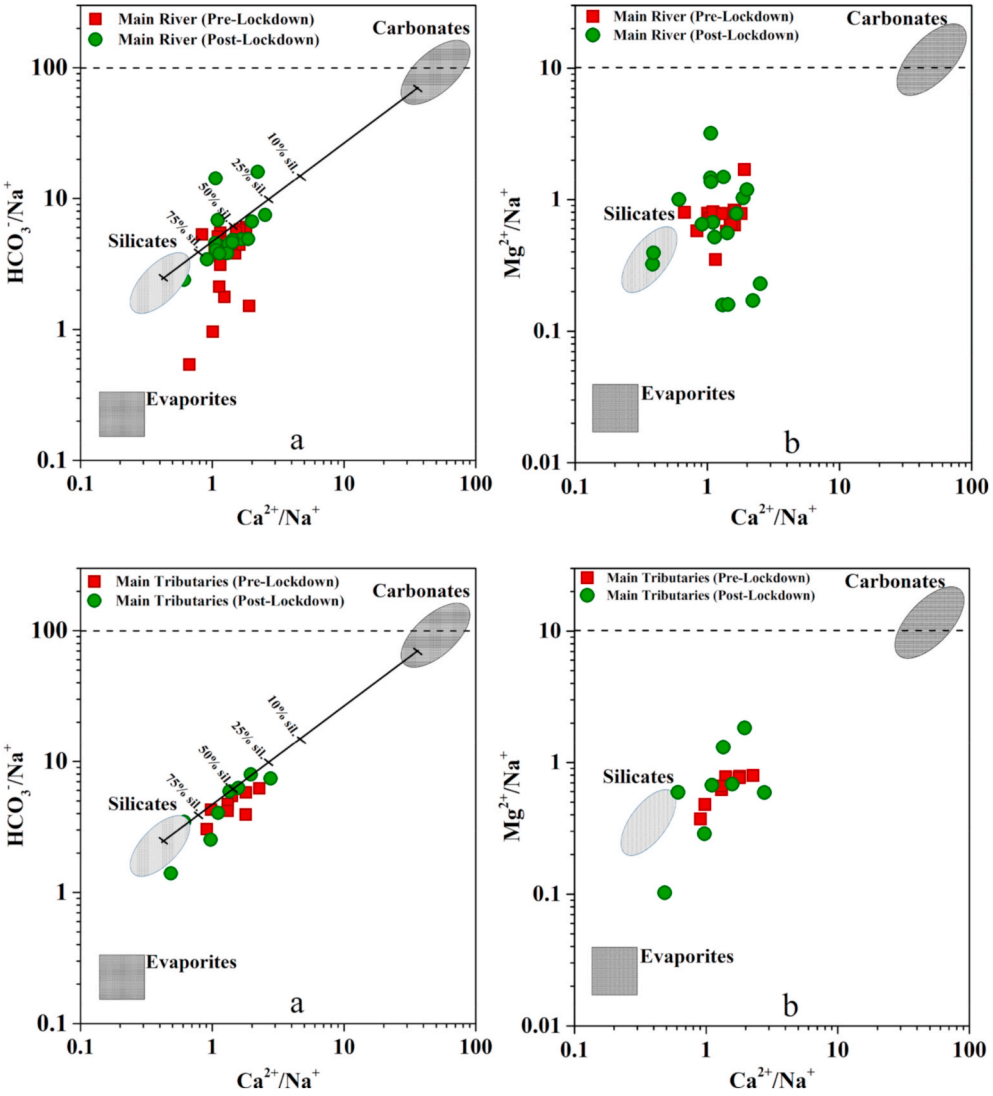

Fig. 8. Mixing diagrams of Na-normalized molar ratios of (a) Ca^{2+} versus HCO_3^- and (b) Ca^{2+} versus Mg^{2+} (pre-lockdown and post-lockdown) in the main river and its tributaries of Bagmati River Basin (BRB), Nepal. The data for carbonates, silicates and evaporates end members are obtained from Gaillardet et al. (1999).

Table 4
Irrigation water quality index depicting the pre-lockdown and post-lockdown scenario in the Bagmati River Basin (BRB), Nepal.

	EC	Na%	SAR	MH	KR	PI	CROSS
BL-Main river	862.57 (E)	36.46 (G)	1.28 (E)	38.15 (S)	0.49(S)	80.32 (Class I)	1.53 (E)
AL-Main river	399.76 (E)	38.04 (E)	1.23 (E)	37.81 (S)	0.56(S)	107.18 (Class I)	1.49 (E)
BL-Tributary	1154.25 (G)	37.82 (G)	1.59 (E)	30.15 (S)	0.52(S)	80.83 (Class I)	1.87 (E)
AL-Tributary	497.38 (E)	40.49 (P)	1.65 (E)	34.82 (S)	0.67(S)	91.27 (Class I)	1.93 (E)

All values derived from (meq/L); E = Excellent, G = Good, P= Permissible, S= Safe, AL = Post-lockdown, BL= Pre-lockdown.

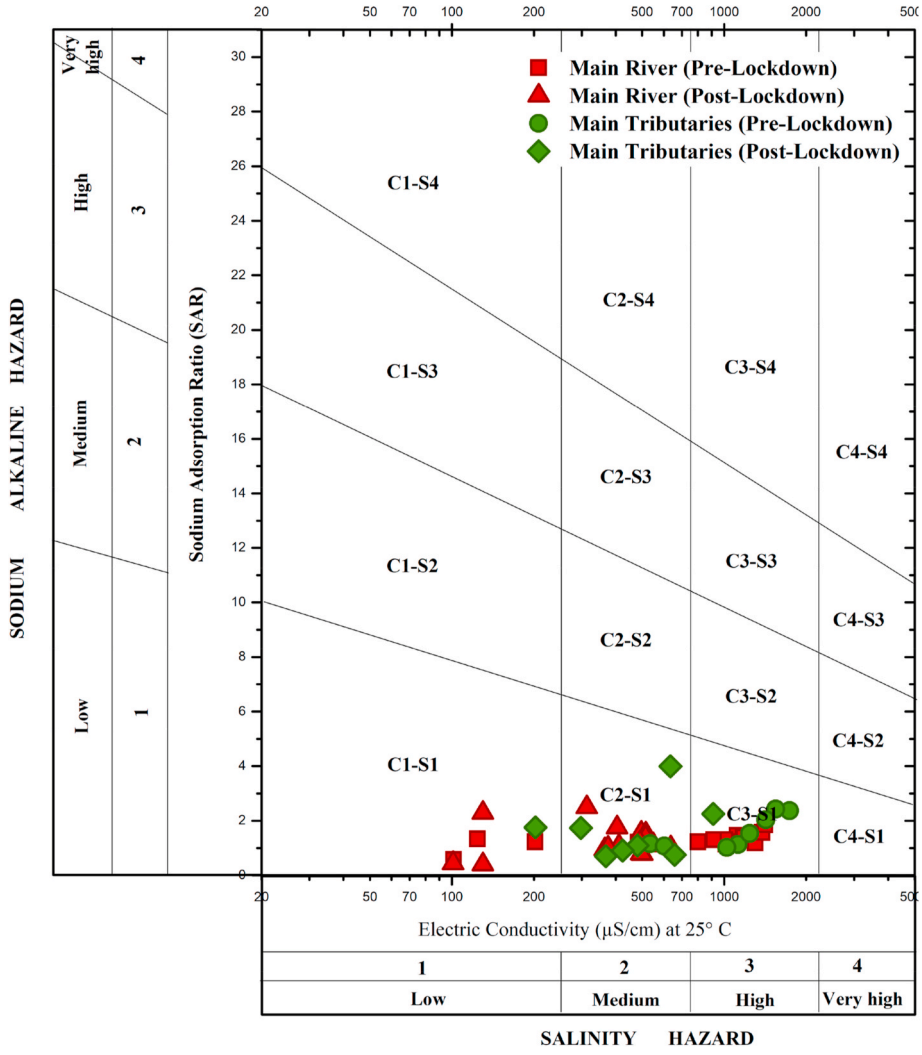

Fig. 9. Wilcox diagram for classifying irrigation water based on sodium adsorption ratio (SAR) in the main river and its tributaries of the Bagmati River Basin (BRB), Nepal.

4. Conclusion

This study evaluated the imprints of lockdown to the Bagmati River Basin (BRB), Nepal with respect to the unprecedented global impacts of the COVID-19 pandemic. The results showed an impressive recovery of the water quality in the BRB during the lockdown phase as compared to the pre-lockdown status. The surface water of the basin was mildly alkaline with moderate EC and TDS indicating low mineralization. The pattern of cationic and anionic dominance in the BRB were:Ca^{2+}> Na^{+}> Mg^{2+}> K^{+}> NH_4^{+} and HCO_3^{-} > Cl^{-}> SO_4^{2-} > NO_3^{-}> PO_4^{3-}, respectively. The hydrochemical facies were found to be Ca–HCO_3 type; however, intense anthropic activities had distinct impacts on the characteristics of the river water. The chemical attributes such as EC, TDS, Ca^{2+}, Na^{+}, NH_4^{+}, and Cl^{-} were significantly decreased during post-lockdown exhibiting the distinct temporal variation mainly due to limited anthropic interferences The multivariate statistical analysis also confirmed the improvement in the water quality of BRB during the lockdown.

Interestingly, the poor water quality changed into relatively better quality in both the main river and tributaries during the post-lockdown but the tributaries showed relatively more deteriorated water quality based on the water quality index. The level of DO was increased ~1.5 times during the post-lockdown, whereas the levels of BOD and COD were decreased by 1.5 and 1.9 times, respectively. The results highlighted the influence of municipal wastage and direct discharge of untreated effluents in the BRB. The results also signify the hydrochemical modifications by anthropic inputs in the BRB due to the lockdown. Similarly, the water quality of BRB was found currently safe in both pre-lockdown and post-lockdown from the irrigational point of view,

however, deteriorating the quality, especially in the tributaries could bring serious implications for the crop and soil productivity. Meanwhile, the drinking water quality index showed that the water is still far away from being potable despite the improvement to some extent during the post-lockdown. Hence, the COVID-19 lockdown acted completely as a ventilator for the restoration of water quality in the BRB. Overall, the quick revival of highly polluted river systems is possible by limiting anthropic interferences. The study also suggested that it is worth controlling the rampant anthropic activities in the vicinity of the river to improve the water quality rather than investing a huge amount of economic resources for the restoration. The findings of the study could be useful to the researchers, policy-makers, and other concerned stakeholders for the sustainable management and restoration of polluted river systems across the globe. Thus, further in-depth research is suggested to ensure the safety and improvement of the water quality in BRB. The findings of the study call for immediate actions against the direct discharge of municipal wastes and untreated effluents into the river water for restoration.

Credit authorship and contribution statement

Ramesh Raj Pant: Conceptualization, Methodology, and first draft preparation; Bhawana Sapkota, Gauri Jayaswal, and Lalit Pathak: Fieldwork, data collection, and laboratory analysis; Khadka Bahadur Pal, Lal B Thapa: Support in fieldwork and draft preparation; Faizan Ur Rehman and Kiran Bishwakarma: Statistical and GIS analysis; Madan Koirala, Kedar Rijal, and Rejina Maskey Byanju: Supervision, review, and editing.

Declaration of competing interest

The authors declare that they have no known competing financial interests or personal relationships that could have appeared to influence the work reported in this paper.

Acknowledgments

This research was supported by the Central Department of Environmental Science, Institute of Science and Technology, Tribhuvan University, Nepal. The authors are obliged to Prof. Dr. Hari Datta Lekhak from Tribhuvan University, Nepal, and Prof. Dr. Zhang Fan from the Institute of Tibetan Plateau Research Chinese Academy of Sciences, China for their comments and suggestions to this research work. Also, we would like to thank Dr. Deep Narayan Shah, Dr. Ram Devi Tachamo Shah, and Mr. Ramesh Basnet for supporting the data collection for this study. Finally, the authors would like to thank the anonymous reviewers for their constructive comments and suggestions which greatly help to polish the manuscript.

Appendix A. Supplementary data

Supplementary data to this article can be found online at https://doi.org/10.1016/j.jenvman.2021.112522.

References

Acharya, A., Sharma, M.L., Bishwakarma, K., Dahal, P., Kumar, S., Chaudhari, Adhikari, B., Neupane, S., Pokhrel, B.N., Pant, R.R., 2020. Chemical characteristics of the karmanasha river water and its appropriateness for irrigational usage. J. Nepal Chem. Soc. 41, 94–102. https://doi.org/10.3126/jncs.v41i1.30494.

Alavi, N., Zaree, E., Hassani, M., Babaei, A.A., Goudarzi, G., Yari, A.R., Mohammadi, M. J., 2016. Water quality assessment and zoning analysis of Dez eastern aquifer by Schuler and Wilcox diagrams and GIS. Desalin. Water Treat. 57, 23686–23697. https://doi.org/10.1080/19443994.2015.1137786.

APHA, 2005. In: Standard Methods for the Examination of Water and Wastewater, twenty-first ed. twenty-first ed. Am. Public Heal. Assoc. Washington. DC, p. 1220. American Public Health Association, Washington DC. Stand. Methods Exam. Water Wastewater.

Bhatnagar, A., Devi, P., George, M.P., 2016. Impact of mass bathing and religious activities on water quality index of prominent water bodies: a multilocation study in Haryana, India. Int. J. Ecol. 2016 https://doi.org/10.1155/2016/2915905.

Bhatt, M.P., Masuzawa, T., Yamamoto, M., Takeuchi, N., 2007. Chemical characteristics of pond waters within the debris area of Lirung Glacier in Nepal Himalaya. J. Limnol. 66, 71–80. https://doi.org/10.4081/jlimnol.2007.71.

Bhatt, M.P., McDowell, W.H., Gardner, K.H., Hartmann, J., 2014. Chemistry of the heavily urbanized Bagmati River system in Kathmandu Valley, Nepal: export of organic matter, nutrients, major ions, silica, and metals. Environ. Earth Sci. 71, 911–922. https://doi.org/10.1007/s12665-013-2494-9.

BIS, 2012. Indian standard drinking water specification (second revision). Bur. Indian Stand. IS 10500, 1–11.

Bishwakarma, K., Pant, R.R., Pal, K.B., Ghimire, A., Thapa, L.B., Saud, P., Joshi, S., Panthi, K.P., 2019. Water quality and land use/cover changes in the Phewa Watershed , Gandaki Province, Nepal. Nepal Journal of Environmental Science 7, 31–39. https://doi.org/10.3126/njes.v7i0.34473.

CBS, 2011. National population and housing census 2011 (national report). Cent. Bur. Stat. 1.

Chaurasia, S., Singh, R., Tripathi, I.P., Ahmad, I., Satna, M.P., 2020. Imprints of COVID -19 Pandemic Lockdown on Water Quality of River Imprints of COVID -19 Pandemic Lockdown on Water Quality of River Mandakini, Chitrakoot.

Corlett, R.T., Primack, R.B., Devictor, V., Maas, B., Goswami, V.R., Bates, A.E., Koh, L.P., Regan, T.J., Loyola, R., Pakeman, R.J., Cumming, G.S., Pidgeon, A., Johns, D., Roth, R., 2020. Impacts of the coronavirus pandemic on biodiversity conservation. Biol. Conserv. 246, 8–11. https://doi.org/10.1016/j.biocon.2020.108571.

Dennison Himmelfarb, C.R., Baptiste, D., 2020. Coronavirus disease (COVID-19). J. Cardiovasc. Nurs. Publish Ah. https://doi.org/10.1097/jcn.0000000000000710.

Diamantini, E., Lutz, S.R., Mallucci, S., Majone, B., Merz, R., Bellin, A., 2018. Driver detection of water quality trends in three large European river basins. Sci. Total Environ. 612, 49–62. https://doi.org/10.1016/j.scitotenv.2017.08.172.

Doneen, L.D., 1954. Salination of soil by salts in the irrigation water. Am. Geophys. Union 35, 3–7.

Dutta, V., Dubey, D., Kumar, S., 2020. Cleaning the River Ganga: impact of lockdown on water quality and future implications on river rejuvenation strategies. Sci. Total Environ. 743, 140756. https://doi.org/10.1016/j.scitotenv.2020.140756.

Fan, B.L., Zhao, Z.Q., Tao, F.X., Liu, B.J., Tao, Z.H., Gao, S., Zhang, L.H., 2014. Characteristics of carbonate, evaporite and silicate weathering in Huanghe River basin: a comparison among the upstream, midstream and downstream. J. Asian Earth Sci. 96, 17–26. https://doi.org/10.1016/j.jseaes.2014.09.005.

Fox, J., Yokying, P., Sharma, N., Chettri, R., 2020. Another Possible Cost of COVID-19: Returning Workers May Lead to Deforestation in Nepal 1–2.

Franch-Pardo, I., Napoletano, B.M., Rosete-Verges, F., Billa, L., 2020. Spatial analysis and GIS in the study of COVID-19. A review. Sci. Total Environ. 140033 https://doi.org/10.1016/j.scitotenv.2020.140033.

Gaillardet, J., Dupré, B., Louvat, P., Allègre, C.J., 1999. Global silicate weathering and CO_2 consumption rates deduced from the chemistry of large rivers. Chem. Geol. 159, 3–30. https://doi.org/10.1016/S0009-2541(99)00031-5.

Ibraheem, A.M., Khan, S.M.M.N., 2017. Suitability Assessment of Groundwater for Irrigation Purpose in Veppanthattai Block, Perambalur District, Tamil Nadu. World Sci. News.

Islam, M.S., Tusher, T.R., Roy, S., Rahman, M., 2020. Impacts of nationwide lockdown due to COVID-19 outbreak on air quality in Bangladesh: a spatiotemporal analysis. Air Qual. Atmos. Heal. https://doi.org/10.1007/s11869-020-00940-5.

Joshi, D.M., Kumar, A., Agrawal, N., 2009. Assessment of the irrigation water quality of river Ganga in Haridwar district. Rasayan J. Chem. 2, 285–292.

Lai, C.C., Shih, T.P., Ko, W.C., Tang, H.J., Hsueh, P.R., 2020. Severe acute respiratory syndrome coronavirus 2 (SARS-CoV-2) and coronavirus disease-2019 (COVID-19): the epidemic and the challenges. Int. J. Antimicrob. Agents 55, 105924. https://doi.org/10.1016/j.ijantimicag.2020.105924.

Lamichhane, S., Shakya, N.M., 2020. Shallow aquifer groundwater dynamics due to land use/cover change in highly urbanized basin: the case of Kathmandu Valley. J. Hydrol. Reg. Stud. 30, 100707. https://doi.org/10.1016/j.ejrh.2020.100707.

Li, S., Xu, Z., Wang, H., Wang, J., Zhang, Q., 2009. Geochemistry of the upper Han River basin, China. 3: anthropogenic inputs and chemical weathering to the dissolved load. Chem. Geol. 264, 89–95. https://doi.org/10.1016/j.chemgeo.2009.02.021.

Mahato, S., Pal, S., Ghosh, K.G., 2020. Effect of lockdown amid COVID-19 pandemic on air quality of the megacity Delhi, India. Sci. Total Environ. 730, 139086. https://doi.org/10.1016/j.scitotenv.2020.139086.

Mehta, K.R., Rana, S.V.S., 2018. Study of physico-chemical parameters of Bagmati River , Kathmandu. Nepal 5, 2042–2048.

Mishra, B.K., Regmi, R.K., Masago, Y., Fukushi, K., Kumar, P., Saraswat, C., 2017. Assessment of Bagmati river pollution in Kathmandu Valley: scenario-based modeling and analysis for sustainable urban development. Sustain. Water Qual. Ecol. 9 (10), 67–77. https://doi.org/10.1016/j.swaqe.2017.06.001.

Murugesan, B., Karuppannan, S., Mengistie, A.T., Ranganathan, M., Gopalakrishnan, G., 2020. Distribution and trend analysis of COVID-19 in India: geospatial approach. J. Geogr. Stud. 1–9 https://doi.org/10.21523/gcj5.20040101.

Pal, K.B., Pant, R.R., Rimal, B., Mishra, A.D., 2019. Comparative assessment of water quality in the Bagmati River basin , Nepal. ZOO-Journal 5, 68–78.

Pant, R.R., Zhang, F., Rehman, F.U., Wang, G., Ye, M., Zeng, C., Tang, H., 2018. Spatiotemporal variations of hydrogeochemistry and its controlling factors in the gandaki river basin, central himalaya Nepal. Sci. Total Environ. 622–623, 770–782. https://doi.org/10.1016/j.scitotenv.2017.12.063.

Pant, R.R., Chalaune, T.B., Dangol, A., Dhital, Y.P., Sharma, M.L., Pal, K.B., Shah, S.T.H., Shrestha, A.K., Thapa, L.B., 2021. Hydrochemical assessment of the Beeshazar and

associated lakes in Central Nepal. SN Appl. Sci. https://doi.org/10.1007/s42452-020-03983-6.
Panthi, J., Dahal, P., Shrestha, M.L., Aryal, S., Krakauer, N.Y., Pradhanang, S.M., Lakhankar, T., Jha, A.K., Sharma, M., Karki, R., 2015. Spatial and temporal variability of rainfall in the gandaki river basin of Nepal himalaya. Climate 3, 210–226. https://doi.org/10.3390/cli3010210.
Paudyal, R., Kang, S., Sharma, C.M., Tripathee, L., Sillanpaä, M., 2016. Variations of the physicochemical parameters and metal levels and their risk assessment in urbanized Bagmati River, Kathmandu, Nepal. J. Chem. 2016 https://doi.org/10.1155/2016/6025905.
Pinder, A.C., Raghavan, R., Britton, J.R., Cooke, S.J., 2020. COVID-19 and biodiversity: the paradox of cleaner rivers and elevated extinction risk to iconic fish species. Aquat. Conserv. Mar. Freshw. Ecosyst. 30, 1061–1062. https://doi.org/10.1002/aqc.3416.
Piper, 1944. A graphic producer in the geochemical interpretation of water analysis. Am. Geophys. Union, pp. 914–928.
Raghunath, H.M., 1987. Ground water. New Age International.
Rengasamy, P., Marchuk, A., 2011. Cation ratio of soil structural stability (CROSS). Soil Res. 49, 280–285. https://doi.org/10.1071/SR10105.
Richards, L.A., 1954. Diagnostics and Improvement of Saline and Alkaline Soils. U.S. Salin. Lab., Washington, DC 0. U.S. Dept. Agric. hand B. no. 600.
Sada, R., 2012. Hanumante River: emerging uses, competition and implications. J. Sci. Eng. 1, 17–24. https://doi.org/10.3126/jsce.v1i0.22489.
Sahu, P., Sikdar, P.K., 2008. Hydrochemical framework of the aquifer in and around East Kolkata Wetlands, West Bengal, India. Environ. Geol. 55, 823–835. https://doi.org/10.1007/s00254-007-1034-x.
Saleh, A., Al-Ruwaih, F., Shehata, M., 1999. Hydrogeochemical processes operating within the main aquifers of Kuwait. J. Arid Environ. 42, 195–209. https://doi.org/10.1006/jare.1999.0511.
Şener, Ş., Şener, E., Davraz, A., 2017. Evaluation of water quality using water quality index (WQI) method and GIS in Aksu River (SW-Turkey). Sci. Total Environ. 584–585, 131–144. https://doi.org/10.1016/j.scitotenv.2017.01.102.
Shah, D.N., Devi, R., Shah, T., Rijal, D., Sharma, S., 2020. Impacts of COVID-19 and Nationwide Lockdown on River Ecosystems in Nepal 56–58. https://doi.org/10.34297/AJBSR.2020.10.001474.Received.
Singh, Y., Khattar, J.I.S., Singh, D.P., Rahi, P., Gulati, A., 2014. Limnology and cyanobacterial diversity of high altitude lakes of Lahaul-Spiti in Himachal Pradesh, India. J. Biosci. 39, 643–657. https://doi.org/10.1007/s12038-014-9458-4.
Singh, V.B., Ramanathan, A.L., Mandal, A., 2016. Hydrogeochemistry of high-altitude lake: a case study of the chandra tal, western himalaya, India. Arab. J. Geosci. 9, 1–9. https://doi.org/10.1007/s12517-016-2358-1.
Thakur, J.K., Neupane, M., Mohanan, A.A., 2017. Water poverty in upper Bagmati River basin in Nepal. Water Sci 31, 93–108. https://doi.org/10.1016/j.wsj.2016.12.001.
Thomas, J., Joseph, S., Thrivikramji, K.P., Manjusree, T.M., Arunkumar, K.S., 2014. Seasonal variation in major ion chemistry of a tropical mountain river, the southern Western Ghats, Kerala, India. Environ. Earth Sci. 71, 2333–2351. https://doi.org/10.1007/s12665-013-2634-2.
Varol, M., Gökot, B., Bekleyen, A., Şen, B., 2013. Geochemistry of the Tigris River basin, Turkey: spatial and seasonal variations of major ion compositions and their controlling factors. Quat. Int. 304, 22–32. https://doi.org/10.1016/j.quaint.2012.12.043.
WHO, 2011. Guidelines for Drinking-Water Quality.
Wilcox, L., 1955. Classification and Use of Irrigation Waters. US Department of Agriculture.
Yunus, A.P., Masago, Y., Hijioka, Y., 2020. COVID-19 and surface water quality: improved lake water quality during the lockdown. Sci. Total Environ. 731, 139012. https://doi.org/10.1016/j.scitotenv.2020.139012.
Zeng, X., Rasmussen, T.C., 2005. Multivariate statistical characterization of water quality in lake lanier, Georgia, USA. J. Environ. Qual. 34, 1980–1991. https://doi.org/10.2134/jeq2004.0337.
Zhang, F., Qaiser, F. ur R., Zeng, C., Pant, R.R., Wang, G., Zhang, H., Chen, D., 2019. Meltwater hydrochemistry at four glacial catchments in the headwater of Indus River. Environ. Sci. Pollut. Res. 26, 23645–23660. https://doi.org/10.1007/s11356-019-05422-5.